

JLAB-THY-99-17
ADP-99-24/T364

FLAVOR ASYMMETRIES IN THE PROTON AND SEMI-INCLUSIVE PROCESSES ^a

W. MELNITCHOUK

*Jefferson Lab, 12000 Jefferson Avenue, Newport News, VA 23606,
and Special Research Centre for the Subatomic Structure of Matter,
University of Adelaide, Adelaide 5005, Australia*

Semi-inclusive electron scattering provides a powerful tool with which to study the spin and flavor distributions in the proton. Greater kinematic coverage at the proposed Electron-Polarized Ion Collider facility will enable the valence d/u ratio to be determined at large x through π^\pm production. At small x , π production can be used to extract the d/\bar{u} ratio, complementing existing semi-inclusive measurements by HERMES, and Drell-Yan data from Fermilab. Asymmetries in heavier quark flavors can also be probed by tagging strange and charm hadrons in the final state.

1 Introduction

Asymmetries in the proton's spin and flavor quark distributions provide direct information on QCD dynamics of bound systems. Difference between quark and antiquark distributions in the sea almost universally signal the presence of phenomena which require understanding of strongly coupled QCD, beyond the realm of perturbation theory. On the other hand, at extreme kinematics at x near unity the x -dependence of quark distributions is determined by perturbative QCD, and can be tested by studying the asymptotic behavior of valence quark distributions.

Most information on quark distributions in the proton to date has come from inclusive scattering, which sums over all charge-squared-weighted flavors. Semi-inclusive scattering, on the other hand, in which a hadron is detected in the final state in coincidence with the scattered lepton, offers considerably more freedom to explore the individual quark flavor content of the nucleon.

In the quark-parton model the cross section for producing a hadron h at a given x and z and large photon virtuality Q^2 can be written (to leading order) as a product of a quark distribution function, $q(x, Q^2)$, and a fragmentation function, $D_q^h(z, Q^2)$, giving the probability of quark q fragmenting into hadron

^aTalk given at the EPIC'99 (Electron-Polarized Ion Collider) Workshop, IUCF, April 1999.

h with a fraction z of the quark's center of mass energy:

$$N^h \sim \sum_q e_q^2 q(x, Q^2) D_q^h(z, Q^2). \quad (1)$$

Here one assumes factorization of the scattering and hadronization processes, which is generally true only at high energy. Recent data from HERMES¹ suggests that the fragmentation functions are, within experimental errors, independent of x , and agree with previous measurements by the EMC² at somewhat larger energies.

2 Current Fragmentation Region

The most direct way to study fragmentation is in the current fragmentation region, in which the observed hadrons are produced (in the photon-hadron center of mass frame) along the direction of the current. Here the photon transfers (hard) momentum to a single parton in the hadron, which is then knocked out and fragments into other hadrons by picking up $q\bar{q}$ pairs from the vacuum. Because it requires only a single $q\bar{q}$ pair, the leading hadrons in this region are predominantly mesons. Furthermore, by studying the fragmentation process at large z , where the knocked out quark is most likely to be contained in the produced meson, one can obtain direct information on the momentum distribution of the scattered quark in the proton. (At small z this information becomes diluted by additional $q\bar{q}$ pairs from the vacuum which contribute to secondary fragmentation.)

2.1 Valence Quark Asymmetries

The valence d/u ratio contains important information about the spin-flavor structure of the proton³. In particular, its asymptotic behavior at large x reflects the mechanism(s) responsible for the breaking of $SU(2)_{\text{spin}} \times SU(2)_{\text{flavor}}$ symmetry. Furthermore, there are firm predictions for this behavior from perturbative QCD⁴, so that measurement of this ratio would be an important indicator of the appropriate kinematics at which QCD can be treated perturbatively.

So far, a direct measurement of d/u has been rather difficult, mainly because the cross sections decrease rapidly in the extreme kinematics near $x \sim 1$. Previous analyses have used inclusive deep-inelastic scattering data on proton and deuteron targets to extract the d/u ratio from the neutron to proton structure function ratio. However, the neutron data suffer from the fact that nuclear effects, even in the deuteron, become quite significant^{5,6} at large x .

In particular, whether one corrects for Fermi motion only, or in addition for binding and nucleon off-shell effects, the extracted neutron structure functions for $x > 0.7$ can differ dramatically⁶. The question is therefore how to avoid uncertainties in the extraction procedure introduced by nuclear effects^{7,8}.

One possibility is to measure the relative yields of π^+ and π^- mesons in semi-inclusive scattering in the current fragmentation region. At large z the u quark fragments primarily into a π^+ , while a d fragments into a π^- , so that at large x and z one has a direct measure of d/u . (Although one should not be too close to $z = 1$, as the fragmentation process there may no longer be incoherent, or factorizable into a partonic cross section and a target-independent fragmentation function.)

The HERMES Collaboration has previously extracted the d/u ratio from the $\pi^+-\pi^-$ difference using both proton and bound neutron targets¹. The advantage of using both p and n is that all dependence on fragmentation functions cancels, removing any uncertainty that might be introduced by incomplete knowledge of the hadronization process. For a proton target one has (dropping the explicit Q^2 dependence):

$$N_p^{\pi^+} \sim 4u(x) D(z) + d(x) \bar{D}(z), \quad (2)$$

$$N_p^{\pi^-} \sim 4u(x) \bar{D}(z) + d(x) D(z), \quad (3)$$

where $D(z) \equiv D_u^{\pi^+} = D_d^{\pi^-}$ is the leading fragmentation function (assuming isospin symmetry), and $\bar{D}(z) \equiv D_d^{\pi^+} = D_u^{\pi^-}$ is the non-leading fragmentation function. With the corresponding expression for a neutron, one can construct a ratio:

$$R_{np}(x, z) \equiv \frac{N_n^{\pi^+} - N_n^{\pi^-}}{N_p^{\pi^+} - N_p^{\pi^-}} = \frac{4d(x)/u(x) - 1}{4 - d(x)/u(x)}, \quad (4)$$

which is then independent of the fragmentation function, and is a function of x only.

The disadvantage of extracting d/u from this ratio is that one must still account for nuclear effects in obtaining $N_n^{\pi^\pm}$ from the proton and deuteron data. The HERMES Collaboration¹ assumed that $N_n^{\pi^\pm} = N_d^{\pi^\pm} - N_p^{\pi^\pm}$. Beyond $x \sim 0.7$, however, the difference between the ratios with $N_n^{\pi^\pm}$ corrected for nuclear effects and that which is not is quite dramatic⁹. Consequently a d/u ratio obtained from such a measurement without nuclear corrections could potentially give misleading results.

One can avoid the problem of nuclear corrections altogether by comparing data for π^+ and π^- production on protons alone. From the ratio of the π^- to

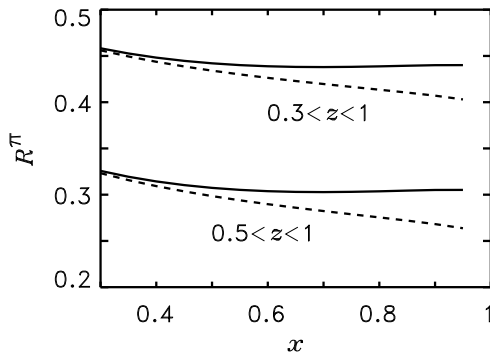


Figure 1: d/u ratio from semi-inclusive π production, for two integration regions, $z > 0.3$ and $z > 0.5$, and for two asymptotic $x \rightarrow 1$ behaviors for d/u : $d/u \rightarrow 0$ (dashed) and $d/u \rightarrow 1/5$ (solid).

π^+ proton cross sections one finds:

$$R^\pi(x, z) \equiv \frac{N_p^{\pi^-}}{N_p^{\pi^+}} = \frac{4\bar{D}(z)/D(z) + d(x)/u(x)}{4 + d(x)/u(x) \cdot \bar{D}(z)/D(z)}. \quad (5)$$

In the limit $z \rightarrow 1$, the leading fragmentation function dominates, $D(z) \gg \bar{D}(z)$, and the ratio $R^\pi \rightarrow (1/4)d/u$. In the realistic case of smaller z , the \bar{D}/D term in R^π contaminates the yield of fast pions originating from struck primary quarks, diluting the cross section with pions produced from secondary fragmentation by picking up extra $q\bar{q}$ pairs from the vacuum. Nevertheless, one can estimate the yields of pions using the empirical fragmentation functions measured by HERMES¹ and the EMC². Integrating the differential cross section over a range of z , as is more practical experimentally, the resulting ratios for cuts of $z > 0.3$ and $z > 0.5$ are shown in Fig. 1 for two different asymptotic $x \rightarrow 1$ behaviors^{3,4,6}: $d/u \rightarrow 0$ (dashed) and $d/u \rightarrow 1/5$ (solid). Decreasing the lower limit for z has the effect of raising the cross section ratio, because of the larger integrated contribution from non-leading fragmentation, which is more important at smaller z . Although the relative difference between the ratios for the two asymptotic d/u behaviors then becomes smaller, the absolute difference between these remains relatively constant, and should be measurable with the high luminosities proposed for EPIC.

2.2 Light Sea Quark Asymmetries

By tagging charged pions produced off protons and neutrons at small x one can also extract information on the flavor dependence of *sea quarks* in the proton. Interest in the proton's \bar{d} and \bar{u} distributions has been renewed recently with the measurement by the E866 Collaboration¹⁰ at Fermilab of the x -dependence of the pd to pp cross section ratio for Drell-Yan production, which is sensitive to \bar{d}/\bar{u} at small and medium x . (Note that nuclear shadowing corrections, which are known to be important in deep-inelastic scattering off the deuteron¹¹ at very small x , are relatively small in the region covered by E866.) Complementary information on this ratio can also be obtained in semi-inclusive scattering by taking the ratio of the isovector combination of cross sections for π^+ and π^- production¹²:

$$\frac{N_p^{\pi^+\pi^-} - N_n^{\pi^+\pi^-}}{N_p^{\pi^+\pi^-} + N_n^{\pi^+\pi^-}} = \frac{3}{5} \left(\frac{u - d - \bar{d} + \bar{u}}{u - d + \bar{d} - \bar{u}} \right) \left(\frac{D + \bar{D}}{D - \bar{D}} \right). \quad (6)$$

The HERMES Collaboration at DESY has in fact recently measured this ratio¹³, although the errors are currently still relatively large compared with the Drell-Yan data¹⁰.

As pointed out by Thomas¹⁴, an excess of \bar{d} quarks in the proton arises naturally from the chiral structure of QCD, in the form of a pion cloud. If part of the proton's wave function can be approximated by a π^+n component, a deep-inelastic probe scattering from the virtual π^+ , which contains a valence \bar{d} quark, will automatically lead to $\bar{d} > \bar{u}$ in the proton. On the other hand, one can also expect the bare nucleon itself (i.e. that which is not dressed by pions) to be asymmetric with respect to its $SU(2)_{\text{flavor}}$ sea. As suggested long ago by Field and Feynman¹⁵, the Pauli exclusion principle can contribute to the asymmetry on the basis of the u and d valence quarks already being unequally represented in the proton.

The x dependence of $\bar{d} - \bar{u}$ provides much more stringent constraints on models of the $SU(2)$ flavor symmetry breaking in the proton sea than earlier measurements¹⁶ which only extracted the first moment of the difference, $\tau = \int_0^1 dx(\bar{d} - \bar{u})$. Analysis¹⁷ of the E866 data suggests that it is rather difficult to ascribe the whole asymmetry over the entire range of x to a single mechanism. On the other hand, Fig. 2 illustrates that a hybrid model, where effects of pions as well as antisymmetrization are taken into account, gives quite a good fit to the data.

The pion cloud contributions are evaluated taking into account both nucleon and Δ recoil states (the latter cancel to some extent the \bar{d} excess through coupling to the $\Delta^{++}\pi^-$ channel). The hadronic form factors, in the \mathcal{M} -

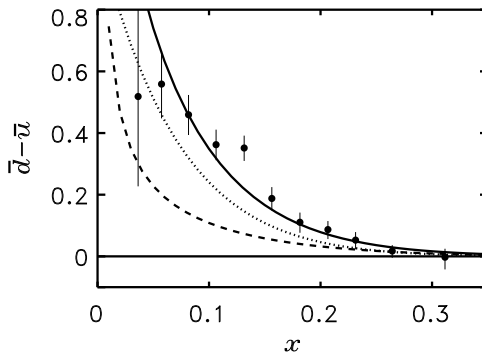


Figure 2: $\bar{d} - \bar{u}$ difference arising from the pion cloud (dashed) and antisymmetrization (dotted) effects, and the combined effect (solid), compared with E866 Drell-Yan data¹⁰.

dependent (light-cone) dipole representation¹⁷ (\mathcal{M} is the invariant mass of the pion-baryon system), are taken to have cut-offs $\Lambda = 1$ GeV and 1.3 GeV for the πN and $\pi N\Delta$ components, respectively. These values, indicating a harder $\pi N\Delta$ contribution than the πNN , are consistent with the measured values of the axial elastic N and $N\Delta$ transition form factors¹⁸.

The contribution from Pauli blocking, which can be parameterized as $(\bar{d} - \bar{u})^{\text{Pauli}} = \tau^{\text{Pauli}}(\alpha + 1)(1 - x)^\alpha$, where α is some large power, is based on MIT bag model calculations¹⁹ which indicate that the normalization, τ^{Pauli} , can be as large as 25%. Phenomenologically, one finds a good fit with $\alpha \approx 14$ and a normalization $\tau^{\text{Pauli}} \approx 7\%$, which is at the lower end of the expected scale but consistent with the bag model predictions¹⁹. Together with the integrated asymmetry from pions, $\tau^\pi \sim 0.05$, the combined value $\tau = \tau^\pi + \tau^{\text{Pauli}} \approx 0.12$ is in quite reasonable agreement with the experimental result, 0.100 ± 0.018 from E866.

Although the presence of an asymmetry is now clearly established, the trend of \bar{d}/\bar{u} at large x , where the cross sections are smaller and errors larger, needs to be confirmed in future experiments. This should provide even stronger constraints on the relative contributions of the pion cloud and antisymmetrization contributions.

2.3 Strange Quark Asymmetries

Asymmetries for light sea quarks are correlated with the valence content of the proton, so that effects of π clouds are difficult to distinguish from those of antisymmetrization. Asymmetries between strange and antistrange quarks, on the other hand, do not suffer from antisymmetrization effects, and therefore give more direct information on the non-perturbative structure of the nucleon sea²⁰.

Evidence for non-perturbative strangeness is currently being sought in a number of processes, ranging from semi-inclusive neutrino induced deep-inelastic scattering to parity violating electron-proton scattering. Perturbative QCD alone generates identical s and \bar{s} distributions, so that any asymmetry would have to be non-perturbative in origin.

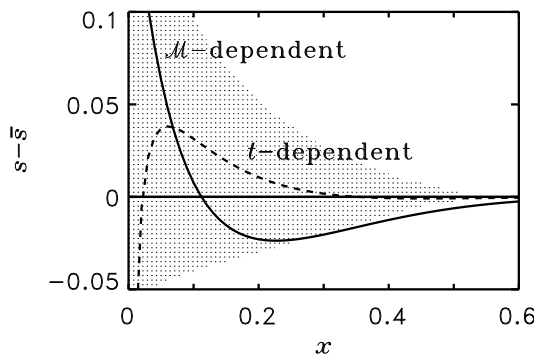


Figure 3: $s - \bar{s}$ difference extracted from ν deep-inelastic data²¹ (shaded), with kaon cloud model predictions for \mathcal{M} -dependent (solid) and t -dependent (dashed) KNY vertex functions with cut-off mass $\Lambda = 1$ GeV.

In deep-inelastic scattering, the CCFR collaboration²¹ analyzed charm production cross sections in ν and $\bar{\nu}$ reactions, which probe the s and \bar{s} distributions in the nucleon, respectively. The resulting difference $s - \bar{s}$, indicated in Fig.3 by the shaded area, has been extracted from the s/\bar{s} ratio and absolute values of $s + \bar{s}$ from global data parameterizations. The curves correspond to chiral cloud model predictions for the asymmetry, in which the strangeness in the nucleon is assumed to be carried by its KY ($Y = \Lambda, \Sigma$) components, so that the s and \bar{s} quarks have quite different origins^{22,23}. Because the s quark originates in the Λ , its distribution is like that of the u quark in the proton, $\sim (1-x)^3$ at large x . The \bar{s} in the kaon, on the other hand, has a much

harder shape, $\sim (1-x)$. In the \mathcal{M} -dependent parameterization of the KNY form factor on the light-cone²⁴ the K distribution in the nucleon is softer than the Λ , thereby compensating somewhat for the harder \bar{s} quark in the K . Nevertheless, for typical form factor cut-offs of $\Lambda \sim 1$ GeV, the softer K distribution in the nucleon is not sufficient to cancel the harder \bar{s} quark in the K , so that the resulting \bar{s} distribution in the nucleon is still bigger than s at large x , as in Fig.3. As a comparison, Fig.3 also shows the asymmetry calculated for a t -dependent KNY form factor²⁴, for which the K distribution in the nucleon is much softer than the Λ , and does in this case overcompensate for the harder \bar{s} distribution in K . However, unlike the light-cone (\mathcal{M} -dependent) forms, the t -dependent form factor introduces additional problems with gauge invariance²⁴.

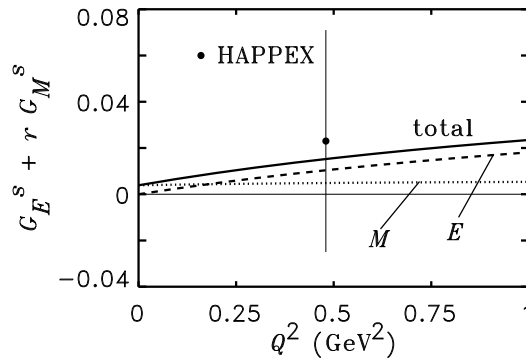


Figure 4: Strange form factor combination measured by the HAPPEX Collaboration²⁶, with kaon cloud predictions for the electric (E) and magnetic (M) contributions, and the total (solid) indicated. For the HAPPEX kinematics $r \approx 0.39$.

Within the same formalism as used to discuss the quark distributions, one can also calculate the strangeness form factors of the nucleon at low Q^2 , which are being measured at MIT-Bates²⁵ and Jefferson Lab²⁶. The latest data on the strange electric and magnetic form factors is shown in Fig.4, together with the kaon cloud predictions, using the same parameters for the KNY couplings and vertex functions as for the $s-\bar{s}$ difference in Fig.3. With a soft KNY form factor the contributions to both G_E^s and G_M^s are small and slightly positive²⁴, in good agreement with the data.

Although the experimental results on non-perturbative strangeness in both structure functions and form factors are still consistent with zero, they are

nevertheless compatible with a soft kaon cloud around the nucleon. New data on $G_{E/M}^s$ from Jefferson Lab with smaller error bars and over a large range of Q^2 will hopefully provide conclusive evidence for the presence or otherwise of a tangible non-perturbative strange component in the nucleon.

2.4 Intrinsic Charm

Extending the above discussion to heavier quarks, one finds that similar relative asymmetries (albeit smaller in magnitude) between c and \bar{c} quarks can also be generated by various non-perturbative mechanisms. Based on some early indications that charm production cross sections in hadronic collisions were larger than predicted by leading order perturbative QCD, Brodsky et al.²⁷ suggested that the discrepancy could be resolved by introducing an intrinsic, non-perturbative, charm component in the nucleon, associated with a higher order, five-quark configuration in the nucleon wave function.

More recently, alternative models for non-perturbative charm have also been proposed^{28,29,30}, in which the charm sea is assumed to arise from the quantum fluctuation of the nucleon to a virtual $D^- \Lambda_c$ configuration, along the lines of the π and K cloud models discussed above. A natural prediction of this model is non-symmetric c and \bar{c} distributions, unlike the five-quark model²⁷ which assumes $c = \bar{c}$. This difference could be tested by comparing charged current events in e^+p and e^-p scattering³⁰.

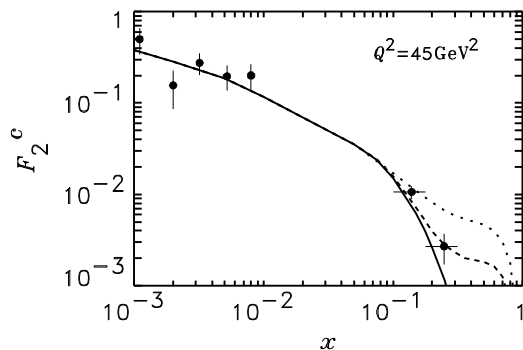


Figure 5: Charm structure function calculated through the interpolating scheme³¹ with different amounts of intrinsic charm: 0% (solid), 0.4% (dashed) and 1% (dotted). The data are from the EMC³².

The most direct information on charm in the nucleon still comes from charm production in deep-inelastic scattering, parameterized by the charm structure function, F_2^c . Since F_2^c receives contributions from both perturbative

and non-perturbative charm, to unambiguously isolate the latter one needs a reliable method of describing perturbative charm generation over a large range of Q^2 , including effects of heavy quark masses and thresholds. Such a scheme was developed recently by Steffens et al.³¹ to smoothly interpolate between the large- Q^2 limit in which massless evolution is applicable, and the low- Q^2 limit where the photon–gluon fusion process is appropriate, and at the same time allow for the presence of non-perturbative charm.

In Fig.5 we show F_2^c calculated using the interpolating scheme³¹ together with different amounts of intrinsic charm from the quantum fluctuation model³⁰, compared with data at large x from the EMC³². The EMC data appear to rule out intrinsic charm at the 1% level, although non-perturbative contributions of order 0.4% are still allowed. More data on the semi-inclusive production of charm at large x would be very valuable in settling the question of the level at which intrinsic charm is present in the nucleon.

3 Target Fragmentation Region

While the hadrons produced in the current fragmentation region are predominantly mesons, the baryon yield in the backward hemisphere of the photon–target center of mass frame, or the target fragmentation region, is observed to be higher by about one order of magnitude. After a collision with a high-energy photon, the remnants of the incident hadron, when viewed in the target rest frame, usually move with small momentum. This makes identification of target fragments in fixed target experiments problematic. On the other hand, a collider set-up such as that envisioned for EPIC, with a high luminosity beam and polarized hadrons, would make the task of studying properties of target fragments considerably easier.

Measurement of baryon fragments in semi-inclusive scattering from hydrogen can provide clear indications of the mechanism underlying the fragmentation process. In fact, the nucleon’s meson cloud gives rise to rather characteristic fragmentation distributions in comparison with the predictions of parton hadronization models, which are significantly enhanced when initial and final state polarization effects are included^{33,34}.

3.1 Kinematics of Target Fragmentation

Consider the semi-inclusive production of a polarized baryon B (with momentum P) from a polarized proton (momentum p), $e\vec{p} \rightarrow e'\vec{B}X$ (the electron can be unpolarized). The four-momentum transfer squared between the initial and final hadrons is $t = (-p_T^2 - (1 - \zeta)(M_B^2 - M^2\zeta))/\zeta$, where $\zeta = p \cdot q / P \cdot q$ is the light-cone fraction of the proton’s momentum carried by the produced

baryon and p_T its transverse momentum. The requirement that the transverse momentum squared of the baryon be positive leads to a kinematic upper limit on t , namely $t_{max} = -(1 - \zeta)(M_B^2 - M^2\zeta)/\zeta$.

For polarized scattering, the proton polarization will be defined to be parallel to the photon direction, and the spin of the produced baryon quantized along its direction of motion. We focus on production of polarized Δ^{++} baryons, rather than for example nucleons, which will reduce backgrounds due to $\Delta \rightarrow N$ decays. Experimentally, the polarization of the produced $\vec{\Delta}^{++}$ can be reconstructed from the angular distribution of its decay products. For the case of $B = \Lambda$, which is relevant when studying the distribution of strangeness in the proton, the polarization of the Λ hyperon will be easier to identify since the Λ is self-analyzing.

3.2 Dynamics of Non-perturbative Sea Generation

In the pion cloud model the differential cross section is determined by the $\pi N \Delta$ vertex function, the pion structure function, and by the amplitude, $T^{s_\Delta s_N}(t)$, for a nucleon of spin s_N to emit a pion with four-momentum squared t , leaving behind a Δ with spin s_Δ . Because it is emitted collinearly (in the target rest frame) with the pion, production of Δ baryons with helicity $\pm 3/2$ is forbidden. The yield of spin projection $\pm 1/2$ states, however, is given by:

$$\mathcal{T}^{+\frac{1}{2} \pm \frac{1}{2}}(t) = \frac{1}{12M_\Delta^2} [(M - M_\Delta)^2 - t] [(M + M_\Delta)^2 - t]^2 (1 \pm \cos \alpha) \quad (7)$$

where α is the angle (in the target rest frame) between the produced baryon and the direction of the photon. With production of Δ baryons limited to forward angles, the factor $(1 \pm \cos \alpha)$ associated with the final state polarization significantly suppresses the $s_\Delta = -1/2$ yield relative to that of $s_\Delta = +1/2$ final states. The spectrum should therefore show strong correlations between the polarizations of the incident proton ($s_N = +1/2$) and the Δ^{++} in the pion exchange model.

A competing process to one pion exchange will be uncorrelated spectator (target remnant, or “diquark” qq) fragmentation. One can estimate the importance of this within the parton model framework³³, in which the differential cross section factorizes into a product of spin-dependent quark distributions and spin-dependent “diquark” fragmentation functions.

In Fig.6 we show the difference $\sigma^{+3/2} - \sigma^{+1/2}$, where $\sigma \equiv Q^2 d^3\sigma/dx dQ^2 d\zeta$, as a fraction of the total spin-averaged cross section, σ_{tot} , for the two models at typical kinematics: $x = 0.075$, $Q^2 = 4 \text{ GeV}^2$ and $\sqrt{s} \approx 8 \text{ GeV}$. For the pion exchange model the form factor cut-off is $\Lambda = 0.8 \text{ GeV}$ (giving an average number density of the $\pi\Delta$ component $\langle n \rangle_{\pi\Delta} \approx 2\%$), although the ratio is almost

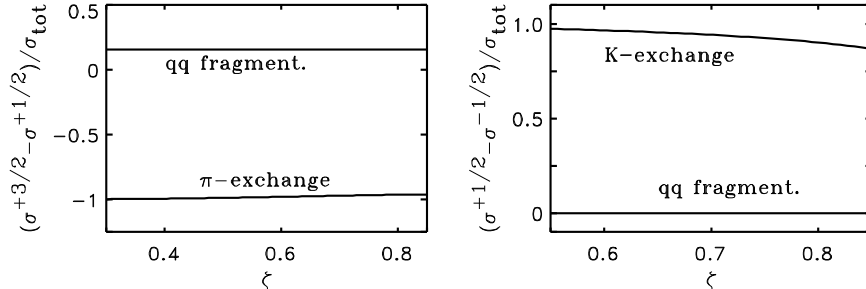


Figure 6: (a) Polarization asymmetry for Δ^{++} production in the π exchange (solid) and qq fragmentation (dashed) models. (b) Asymmetry for Λ production in the K exchange (solid) and qq fragmentation (dashed) models.

insensitive to the size of the form factor cut-off. For the $qq \rightarrow \Delta$ fragmentation functions we use empirical information on unpolarized qq fragmentation together with SU(6) relations for the spin dependence³³. The resulting ζ distributions are almost flat, but dramatically different for the two models. In particular, the pion model predicts a large *negative* asymmetry, while the asymmetry in the qq fragmentation model is small and *positive*.

Similarly, a kaon cloud model predicts the initial proton and recoil Λ polarizations to be very strongly correlated, so that the asymmetry in Fig.6 for the cross sections is almost unity. The K exchange ratios are very similar to the π exchange results, indicating the similar spin transfer dynamics inherent to the meson cloud picture of the nucleon. This is in strong contrast with the expectation from $qq \rightarrow \Lambda$ diquark fragmentation, in which the initial-final state spin correlation is much weaker. In fact, since the probabilities to form a Λ^\uparrow and Λ^\downarrow from an uncorrelated qq pair are equal, in the leading fragmentation approximation the asymmetry will be zero. Of course, SU(6) symmetry breaking effects, as well as non-leading fragmentation contributions, will modify this result, as will contributions from the production and decay of $\Sigma^{0\uparrow\downarrow}$ hyperons. However, the qualitative result that the asymmetry is small should remain true.

Of course the model curves in Fig.6 represent extreme cases, in which the Δ (Λ) baryons are produced entirely via π (K) emission or qq fragmentation, with no interference effects between them. In reality one can expect experimental

asymmetries to lie somewhere between the two limits. The amount of deviation from the parton model curve will indicate the extent to which the meson-exchange process is relevant. Unlike inclusive deep-inelastic scattering, which can only be used to place upper bounds on the pion density¹⁴, the semi-inclusive measurements could pin down the absolute value of $\langle n \rangle_{\pi\Delta}$ ($\langle n \rangle_{K\Lambda}$).

4 Conclusion

In summary, semi-inclusive scattering offers unique opportunities for probing the spin and flavor structure of the nucleon not available with inclusive processes. The polarized electron-hadron collider set-up proposed at EPIC would allow new regions of kinematics to be accessed in which the dynamics of strongly interacting QCD can be probed.

We have outlined a number of specific examples where measurement of asymmetries in the nucleon's valence and sea quark distributions can reveal hitherto hidden details of the non-perturbative structure of the nucleon. The ratio of the valence d/u quarks at large x , which reflects the mechanism of $SU(2)_{\text{spin}} \times SU(2)_{\text{flavor}}$ symmetry breaking, can be determined by tagging pions⁹ in the current fragmentation region at large z . Existing measurements of the neutron/proton structure function ratio, from which d/u is usually extracted, are plagued by large nuclear binding and Fermi motion effects⁶ in the deuteron in the region $x \approx 1$.

Pion production can also be used to pin down the ratio of the \bar{d}/\bar{u} distributions at small and medium x . This can provide constraints on models which attempt to describe the non-perturbative generation of the sea, for example in terms of a chiral cloud of mesons around the nucleon^{14,17}. Measurements of the light antiquark asymmetry can also be correlated with similar asymmetries for strange and even charm quarks and antiquarks, where effects of antisymmetrization are no longer present.

The major advantage in studying semi-inclusive processes with a polarized collider will be in the target fragmentation region. As well as allowing the problem of spectator fragmentation to be tackled seriously for the first time, careful measurements of polarized baryon remnants from polarized protons could enable one to unambiguously establish the magnitude of a pion and kaon cloud of the nucleon at high energies³³. While the experiments proposed are difficult, requiring all the intensity and duty factor one can obtain at EPIC, it does open the way for studying the non-perturbative structure of the nucleon in previously unexplored terrain.

Acknowledgments

I would like to thank the organizers of the EPIC'99 Workshop and the IUCF for their hospitality and support, and travel support from the Forschungszentrum Jülich. I am indebted to M. Malheiro, J. Speth, F.M. Steffens and A.W. Thomas for their collaboration on much of the work presented here.

References

1. K. Ackerstaff, First Results from the HERMES Experiment using Unpolarized Targets, PhD thesis, Univ. Hamburg, 1996.
2. J.J. Aubert et al., Nucl. Phys. B213 (1983) 213.
3. N. Isgur, Phys. Rev. D 59 (1999) 034013.
4. G.R. Farrar and D.R. Jackson, Phys. Rev. Lett. 35 (1975) 1416.
5. W. Melnitchouk, A.W. Schreiber and A.W. Thomas, Phys. Lett. B 335 (1994) 11; Phys. Rev. D 49 (1994) 1183.
6. W. Melnitchouk and A.W. Thomas, Phys. Lett. B 377 (1996) 11.
7. W. Melnitchouk and J.C. Peng, Phys. Lett. B 400 (1997) 220.
8. W. Melnitchouk, M. Sargsian and M.I. Strikman, Z. Phys. A 359 (1997) 99.
9. W. Melnitchouk, J. Speth and A.W. Thomas, Phys. Lett. B 435 (1998) 420.
10. E.A. Hawker et al., Phys. Rev. Lett. 80 (1998) 3715.
11. W. Melnitchouk and A.W. Thomas, Phys. Rev. D 47 (1993) 3783.
12. J. Levelt, P.J. Mulders and A.W. Schreiber, Phys. Lett. B 263 (1991) 498.
13. K. Ackerstaff et al., Phys. Rev. Lett. 81 (1998) 5519.
14. A.W. Thomas, Phys. Lett. B 126 (1983) 97; see J. Speth and A.W. Thomas, Adv. Nucl. Phys. 24 (1998) 83, for a review.
15. R.D. Field and R.P. Feynman, Phys. Rev. D 15 (1977) 2590.
16. M. Arneodo et al., Phys. Rev. D 50 (1994) 1.
17. W. Melnitchouk, J. Speth and A.W. Thomas, Phys. Rev. D 59 (1999) 014033.
18. T. Kitagaki et al, Phys. Rev. D 42 (1990) 1331.
19. A.I. Signal and A.W. Thomas, Phys. Lett. B 211 (1988) 481; A.I. Signal and A.W. Thomas, Phys. Rev. D 40 (1989) 2832; A.W. Schreiber, A.I. Signal and A.W. Thomas, Phys. Rev. D 44 (1991) 2653.
20. X. Ji and J. Tang, Phys. Lett. B 362 (1995) 182.
21. A.O. Bazarko et al., Z. Phys. C 65 (1995) 189.
22. A.I. Signal and A.W. Thomas, Phys. Lett. 191 B (1987) 205.
23. P. Geiger and N. Isgur, Phys. Rev. D 55 (1997) 299.

24. W. Melnitchouk and M. Malheiro, Phys. Lett. B 451 (1999) 224; Phys. Rev. C 55 (1997) 431; Phys. Rev. C 56 (1997) 2373.
25. B. Mueller et al., Phys. Rev. Lett. 78 (1997) 3824.
26. K.A. Aniol et al., Phys. Rev. Lett. 82 (1999) 1096.
27. S.J. Brodsky, P. Hoyer, C. Peterson and N. Sakai, Phys. Lett. 93 B (1980) 451.
28. F.S. Navarra, M. Nielsen, C.A.A. Nunes and M. Teixeira, Phys. Rev. D 54 (1996) 842.
29. S.J. Brodsky and B.Q. Ma, Phys. Lett. B 381 (1996) 317.
30. W. Melnitchouk and A.W. Thomas, Phys. Lett. B 414 (1997) 134.
31. F.M. Steffens, W. Melnitchouk and A.W. Thomas, hep-ph/9903441.
32. J.J. Aubert et al., Nucl. Phys. B213 (1983) 31.
33. W. Melnitchouk and A.W. Thomas, Proceedings of the Workshop on CEBAF at Higher Energies, Newport News, Virginia (1994), nucl-th/9410018.
34. W. Melnitchouk and A.W. Thomas, Z. Phys. A 353 (1995) 311.